Rend. Istit. Mat. Univ. Trieste
Volume 52 (2020), 7–25
DOI: 10.13137/2464-8728/30761

Complicated dynamics in a model of charged particles

Oltiana Gjata and Fabio Zanolin

"Dedicated to Professor Julián López-Gómez for his 60th birthday"

Abstract. *We give an analytical proof of the presence of complex dynamics for a model of charged particles in a magnetic field. Our method is based on the theory of topological horseshoes and applied to a periodically perturbed Duffing equation. The existence of chaos is proved for sufficiently large, but explicitly computable, periods.*

Keywords: Hamiltonian systems, period map, saddle points, homoclinic solutions, chaotic dynamics, topological horseshoes.
MS Classification 2010: 34C25, 34B18, 34C35.

1. Introduction

Recent numerical studies in [5] have shown chaotic aspects in a model describing the motion of charged particles inside a tokamak magnetic field.

A tokamak is a device, invented in the 1950s by the Soviet physicists Sakharov and Tamm, which employs a powerful magnetic field to confine hot plasma in the shape of a torus and keep it away from the machine walls. At the current stage of scientific knowledge and engineering capabilities, tokamaks are still considered among the most promising devices for a possible future production of energy through controlled atomic fusion. From this point of view, the study of mathematical and physical models describing the motion of charged particles inside toroidal (or cylindrical) magnetic fields like those generated by the tokamak coils is of great significance for the possible applications to plasma physics. In the recent past, periods of great expectation on the possibility of obtaining a stable controlled nuclear fusion process using the tokamaks were followed by periods of disappointment for the failure of some critical experiments. This happened due to the discovery of several new and unexpected instability phenomena that have compromised the performance of the device, including dangerous fluctuations of the plasma going in contact with the walls of the reactor. The sensitive dependence on initial conditions is one of the typical instability phenomena appearing in connection with so-called "chaotic behav-

ior". Although stable and random motions can coexist and thus the presence of some chaotic dynamics may be compatible with results about the boundedness of the solutions, nevertheless in many cases (typical examples come from celestial mechanics, see [9, Introduction]) small instability effects due to chaos phenomena may produce relevant long term consequences. From this point of view, investigating the possibility of chaos in differential equations models for tokamak magnetic confinement, is not only a topic with its own theoretical interest, but it may also suggest some possible issues to be taken into account by the scientists involved in the design of these devices.

In [5] the Authors have considered two different configurations leading to Hamiltonian chaos for charged particle motions in a toroidal magnetic field. In the (r, θ, ϕ) coordinates for the torus (cf. [5, Fig. 1]) the tokamak magnetic field has the following form

$$\mathbb{B} = \frac{B_0 R}{\xi}(\hat{\mathbf{e}}_\phi + f(r)\hat{\mathbf{e}}_\theta), \tag{1}$$

where $\xi = R + r\cos(\theta)$ and $\hat{\mathbf{e}}_\phi$, $\hat{\mathbf{e}}_\theta$ are the unit vectors associated respectively with the ϕ and θ directions. The toroidal component along $\hat{\mathbf{e}}_\phi$ depends upon the external magnetic field generated by the coils around the device. The constant B_0, according to [5] is the typical magnetic intensity at the center of the torus. If the plasma is present, a generated current inside the tokamak leads to the creation of a poloidal component for the magnetic field, expressed by the term $f(r)\hat{\mathbf{e}}_\theta$ [1].

In a recent paper [7], we have examined the first configuration considered by the Authors in [5], namely the case in which the poloidal component is negligible. This situation is useful for the study of the motion on an hypothetic single charged particle inside the tokamak with no plasma inside.

In the present article we focus our attention to the second case discussed in [5] in which the effect of the plasma is substantial. In order to simplify the model, in [5, Section C and IV] the Authors consider a cylindrical magnetic geometry, which is the limit, when R tends to infinity, of the toroidal system. In this approximation, the direction $\hat{\mathbf{e}}_\phi$ becomes a stationary vector, subsequently identified to the z-component. In this manner, instead of an empty toroidal solenoid, we are led now to consider a cylindrical plasma tube. An application of Newton law to a charged particle of mass m and charge q moving in this magnetic field (see Section 2 for the details), leads to an integrable system with an associated effective Hamiltonian of the form

$$H_{eff} = \frac{m\dot{r}^2}{2} + \frac{mA^2}{2r^2} + \frac{(qB_0)^2}{8m}r^2 + \frac{q^2}{2m}F^2(r), \quad r > 0, \tag{2}$$

[1] The terms "toroidal" and "poloidal" refer to directions relative to a torus of reference. The poloidal direction follows a small circular ring around the surface, while the toroidal direction follows a large circular ring around the torus (according to Wikipedia). The introduction of these terms comes from [6] for the study of the Earth's magnetic field.

where A is a positive constant and $F(r) = \int^r f(x)\,dx$ (see [5, Appendix B]). Clearly the choice of f and then F greatly influences the Hamiltonian and hence the corresponding dynamics of the particles.

Writing (2) in a dimensionless form and deriving the corresponding differential equation for the new variable $x := r > 0$, we find that the trajectories of the charged particles can be described by a second-order Duffing equation

$$\ddot{x} + g(x) = 0$$

with a singularity at the origin. In [5] the Authors propose a mechanism to produce chaotic dynamics by a perturbation of (2). More precisely, the constant A in (2) (indicated in [5] by C'' in the dimensionless version of H_{eff}) is now considered as a slowly time dependent variable. Numerical evidence of chaos for the stroboscopic (Poincaré) map is provided by the analysis of the Poincaré section. Inspired by this example, we try to analyze this problem with a different approach, by considering a time-periodic perturbation of the associated Duffing equation. Our perturbation can be produced either by a slow modification of the constant A as in [5] o, by modifying the magnetic intensity B_0 . In each case, we produce chaotic dynamics by assuming that a formerly presumed constant coefficient in (2) becomes a slowly varying stepwise periodic function. The choice of a stepwise function (following [11, 12]) has the advantage that the corresponding differential equation system becomes a switched system for which we can apply recent results from the theory of topological horseshoes and therefore we can give a rigorous analytical proof of the existence of chaos.

In our investigation and following [5], we assume for the function F (the primitive of the amplitude of the poloidal field), the expression

$$F(x) := ax^2 \exp\left(-\frac{x^2}{c^2}\right),$$

where $a, c > 0$ are suitable constants. With such a choice of the function F and tuning suitably the constants a and c (the Authors in [5] provide physically meaningful values for these constants), we can produce, for the planar system

$$\dot{x} = y, \qquad \dot{y} = -g(x),$$

a phase-portrait which consists of two local centers surrounded by periodic orbits of increasing period and bounded by two homoclinic trajectories departing from an intermediate saddle point, thus altogether shaping a typical eight figure. After a small perturbation of the magnetic field we obtain another eight shaped figure which partially overlaps with the previous one. Near the intersections of the homoclinic trajectories associated with the two portraits we can define some appropriate rectangular regions where we can prove the existence

of chaos on m-symbols ($m \geq 2$), for the Poincaré map, using the "stretching along the paths" (SAP) technique [13, 17]. It is well known that for periodic planar systems obtained as a perturbation of an autonomous system with a homoclinic orbit at a saddle point, the Melnikov method (see [8]) is a powerful tool to verify the existence of chaotic dynamics. Relevant developments for periodically perturbed Duffing equations are given in [3, 15]. In the applications of the Melnikov method one has to prove the existence of simple zeros for suitable integrals depending on the explicit analytical expression of the homoclinic solution. Unfortunately, in our example, such analytical expression is not available and this motivates the use of a different approach.

The plan of the paper is the following. In Section 2 we briefly describe the mathematical model considered in [5] in order to give a physical justification about the Hamiltonian defined in (2). In Section 3 we choose a special form for $F(x)$ (as proposed in [5]) which produces a double well potential in H_{eff}. Next in the same section, we also discuss the corresponding phase-portrait for the associated Duffing equation and then, as a further step, we introduce the time-periodic perturbation on the differential equation and define six rectangular regions where we will focus our analysis for the SAP technique. Section 4 contains our main result about chaotic dynamics whose proof is finally given in the subsequent Section 5.

2. Mathematical model

We follow the calculations in [5, Appendix B], in order to introduce the mathematical model that we are going to study. In [5] the Authors introduce a cylindrical magnetic geometry, which is considered as the limit, when R tends to infinity, of the toroidal system. The approximation to new geometric configuration leads to a magnetic field rewritten as

$$\mathbb{B} = B_0 \hat{\mathbf{e}}_z + f(r)\hat{\mathbf{e}}_\theta.$$

This is derived in [5] from (1) as a limit for $R \to \infty$ and considering the z-direction identified with the axes along with $\hat{\mathbf{e}}_\phi$, which is considered now as a constant. In order to avoid misunderstanding, it is important to notice (cf. [5, Appendix B]) that the z-direction here is not the one considered originally in [5, Fig. 1]. Moreover, with respect to (1), now the function f already incorporates the effect of B_0 .

In order to find the differential system describing the dynamics of the particle of mass m and charge q moving in this magnetic field, we use the fact that the force acting on the charged particle is given by $\mathbf{F} = q\vec{v} \wedge \mathbb{B}$ (where $\vec{v}$ is the velocity of the particle). Next we recall also the expressions of the velocity and the acceleration in cylindrical coordinates, namely

$$\vec{v} = \dot{r}\hat{\mathbf{e}}_r + r\dot{\theta}\hat{\mathbf{e}}_\theta + \dot{z}\hat{\mathbf{e}}_z$$

and

$$\vec{a} = (\ddot{r} - r\dot{\theta}^2)\hat{\mathbf{e}}_r + (r\ddot{\theta} + 2\dot{r}\dot{\theta})\hat{\mathbf{e}}_\theta + \ddot{z}\hat{\mathbf{e}}_z.$$

Then, an application of the Newton second law, yields to

$$\begin{cases} \ddot{r} - r\dot{\theta}^2 = \frac{q}{m}(B_0 r\dot{\theta} - f(r)\dot{z}) \\ r\ddot{\theta} + 2\dot{r}\dot{\theta} = -\frac{qB_0}{m}\dot{r} \\ \ddot{z} = \frac{q}{m}\dot{r}f(r) \end{cases} \tag{3}$$

Multiplying by r the second equation and then integrating the second and the third equations, we obtain

$$\begin{cases} \dot{\theta} = \frac{A}{r^2} - \frac{qB_0}{2m} \\ \dot{z} = \frac{q}{m}F(r) \end{cases} \tag{4}$$

where A is a constant and $F(r) = \int^r f(x)dx$. Substituting the two equations of (4) into the first equation of (3), we obtain the second-order ODE

$$\ddot{r} - \frac{A^2}{r^3} + \left(\frac{qB_0}{2m}\right)^2 r + \frac{q^2}{m^2}f(r)F(r) = 0. \tag{5}$$

Multiplying equation (5) by $\dot{r}$ and then integrating we finally obtain

$$\int \dot{r}\ddot{r}dt - \int_{r=r(t)} \frac{A^2}{r^3}dr + \left(\frac{qB_0}{2m}\right)^2 \int_{r=r(t)} r dr + \frac{q^2}{m^2}\int_{r=r(t)} F(r)F'(r)dr = \text{constant}.$$

Thus we end up with an effective Hamiltonian, which is precisely the one considered in (2), namely

$$H_{eff} := \frac{m\dot{r}^2}{2} + \frac{mA^2}{2r^2} + \frac{(qB_0)^2}{8m}r^2 + \frac{q^2}{2m}F^2(r).$$

3. Geometric configurations

Following [5] we consider now the effective Hamiltonian

$$H_{\text{eff}} := \frac{\dot{r}^2}{2} + \frac{A^2}{2r^2} + \frac{B_0^2}{8}r^2 + F^2(r) \tag{6}$$

for

$$F(r) := ar^2 \exp\left(-\frac{r^2}{c^2}\right), \tag{7}$$

where A, a, c are suitable positive constants and B_0 is the intensity (magnitude) of the magnetic field. Without loss of generality, we have considered in (6) a unitary mass m and a unitary charge q (cf. formula $(B7)$ in [5]). According to (2), the term depending on $f(r)$ should be of the form $F^2(r)/2$, but clearly there is no mistake in replacing it with $F^2(r)$ (just rename the original function f or replace a with $a\sqrt{2}$ in (7)). As in [5] we assume that the constants in the function F are adjusted in order to generate a double well potential in the effective Hamiltonian. We split H_{eff} as

$$H_{\text{eff}} = E_c + V_0(r) + F^2(r),$$

where E_c, is the kinetic energy and V_0 is the potential in absence of the component of the magnetic field given by $f(r)$. To explain the details, the potential $V_0(r)$ tends to infinity for $r \to 0^+$ and $r \to +\infty$ and it has a unique point of minimum at $r_0 > 0$, where $r_0^2 := 2A/B_0$. In [5], the Authors propose to fix the parameters a and c for the function F in order to produce a maximum point near r_0, so that the new potential $V_0(r) + F^2(r)$ assumes a double-well shape as in Figure 1 below. This is obtained by choosing c^2 close to r_0^2 and $a > 0$ sufficiently large.

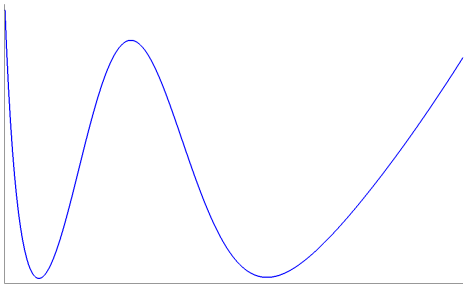

Figure 1: A possible profile of the modified potential $V_0(r) + F^2(r)$ for $r > 0$. The coefficients are tuned-up with a choice of $c^2 > r_0^2$.

The level lines of the effective Hamiltonian function in the right half-plane $\mathbb{R}_0^+ \times \mathbb{R}$ describe a phase-portrait with two centers separated by homoclinic orbits emanated from an intermediate saddle point. The typical portrait is like in Figure 2.

The level lines of H_{eff} are associated with the orbits of the second-order Duffing equation

$$\ddot{x} + g(x) = 0, \tag{8}$$

or, equivalently, the planar conservative system

$$\begin{cases} \dot{x} = y \\ \dot{y} = -g(x), \end{cases} \tag{9}$$

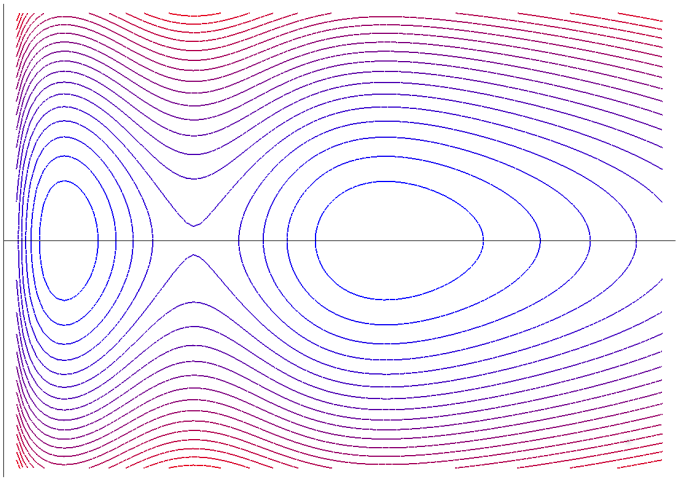

Figure 2: Some level lines associated with the Hamiltonian H_{eff} in the plane $(r, \dot{r})$ for $r > 0$.

for $x := r > 0$, $y = \dot{r}$ and

$$g(x) := \frac{d}{dx}\left(V_0(x) + F(x)^2\right) = -\frac{A^2}{x^3} + \frac{{B_0}^2}{4}x + 2F(x)f(x), \tag{10}$$

where we have set

$$f(x) := F'(x).$$

If we choose F in order to produce a potential as described in [5, Section IV] and in Figure 1, we find that the map g has precisely three simple zeros for $x > 0$ that we denote and order as

$$a < x_s < b.$$

In the phase-plane $\mathbb{R}_0^+ \times \mathbb{R}$, the points $(a, 0)$ and $(b, 0)$ are local centers, while $(x_s, 0)$ is a saddle point.
The level line of the Hamiltonian/energy function (from now on denoted simply by H) passing through $(x_s, 0)$ is given by

$$H(x, y) := \frac{y^2}{2} + V_0(x) + F^2(x) = c_s := V_0(x_s) + F^2(x_s).$$

Such level line is a double homoclinic loop, namely, it splits as

$$\mathcal{O}_l \cup \{(x_s, 0)\} \cup \mathcal{O}_r\,,$$

where $\mathcal{O}_l$ and $\mathcal{O}_r$ two homoclinic orbits at the saddle point $\{(x_s,0)\}$. By convention, we suppose that $\mathcal{O}_l$ is contained in the strip $0<x<x_s$ and surrounds $(a,0)$, while $\mathcal{O}_r$ is contained in the half-plane strip $x>x_s$ and surrounds $(b,0)$. We denote by $(\underline{a},0)$ and the $(\underline{b},0)$ the intersection points of $\mathcal{O}_l$ and, respectively, $\mathcal{O}_r$ with the x-axis. By definition, we have

$$0<\underline{a}<a<x_s<b<\underline{b},$$

with $\underline{a}, x_s, \underline{b}$ the three solutions of $V_0(x)+F^2(x)=c_s$ (see Figure 1).
We also introduce the open regions

$$\mathcal{W}_l := \{(x,y) : 0<x<x_s\,,\ H(x,y)<c_s\}$$

and

$$\mathcal{W}_r := \{(x,y) : x>x_s\,,\ H(x,y)<c_s\}.$$

By construction, we have

$$\partial\mathcal{W}_l = \mathcal{O}_l\cup\{(x_s,0)\} \quad \text{and} \quad \partial\mathcal{W}_r = \mathcal{O}_r\cup\{(x_s,0)\}$$

(see Figure 3).

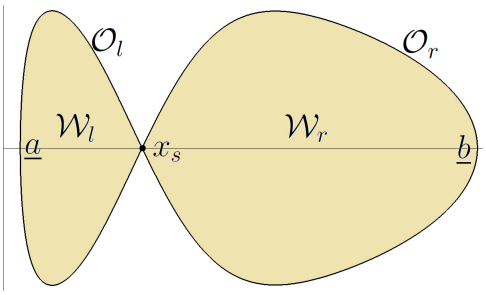

Figure 3: The saddle point $(x_s,0)$ with the homoclinic orbits $\mathcal{O}_l, \mathcal{O}_l$ and the resulting regions $\mathcal{W}_l, \mathcal{W}_l$.

As a next step, we suppose that the modulus of the magnetic field B_0 is effected by a small change so that the three equilibrium points $(a,0), (x_s,0)$ and $(b,0)$ are shifted along the x-axis. We suppose that the effect is small enough so that the new point $(x_s,0)$ will belong to the region surrounded by $\mathcal{O}_l$ or the one surrounded by $\mathcal{O}_r$. More precisely, if we denote by $B_0^{(1)}$ and $B_0^{(2)}$ two different values of the magnetic field and associated the index $i=1,2$ to the corresponding equilibrium points and homoclinic orbits, we will assume that

$$H^{(1)}(x_s^{(2)},0)<H^{(1)}(x_s^{(1)},0) \quad \text{and} \quad H^{(2)}(x_s^{(1)},0)<H^{(2)}(x_s^{(2)},0). \tag{11}$$

We tacitly use the convention that the apex $i = 1, 2$ is associated to the points, orbits and regions of the phase-plane associated with the differential systems having Hamiltonians $H^{(1)}$ and $H^{(2)}$ for the magnetic fields $B_0^{(1)}$ and $B_0^{(2)}$. Under the assumption (11) the homoclinic loops associated with the two Hamiltonian systems, overlap as in Figure 4.

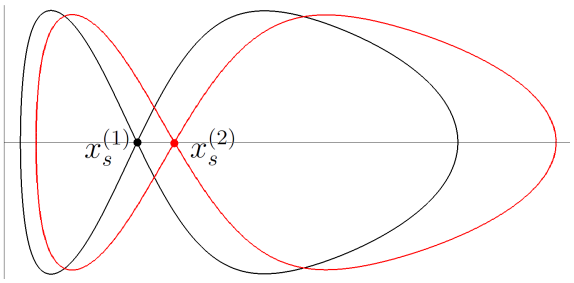

Figure 4: An example of the double homoclinic loops overlapping. The effect is obtained by moving the saddle point x_s. This occurs via a change of parameters in the equation. The aspect/ratio has been slightly modified in order to make the overlapping more evident.

Our plan is to construct some regions homeomorphic to rectangles which are obtained as intersections of suitable narrow bands around the homoclinics.

Let us consider the level line $H^{(1)}(x, y) = c^{(1)}$ with $c^{(1)} < H^{(1)}(x_s^{(1)}, 0)$ and $H^{(1)}(x_s^{(1)}, 0) - c^{(1)}$ small enough. This level line splits into two components, which are contained in the open regions $\mathcal{W}_l^{(1)}$ and $\mathcal{W}_r^{(1)}$, respectively. Now the equation $V_0(x) + F^2(x) = c^{(1)}$ has four solutions that we will denote $a_\pm^{(1)}$ and $b_\pm^{(1)}$, so that

$$\underline{a}^{(1)} < a_-^{(1)} < a^{(1)} < a_+^{(1)} < x_s^{(1)} < b_-^{(1)} < b^{(1)} < b_+^{(1)} < \underline{b}^{(1)} .$$

For the system associated with $B_0^{(2)}$, we can similarly determine some corresponding points with

$$\underline{a}^{(2)} < a_-^{(2)} < a^{(2)} < a_+^{(2)} < x_s^{(2)} < b_-^{(2)} < b^{(2)} < b_+^{(2)} < \underline{b}^{(2)} .$$

By suitably selecting the energy levels, it is always possible to enter in a setting such that the *crossing condition*

$$(CC) \qquad \begin{array}{lll} a_-^{(1)} < & \underline{a}^{(2)} < a_-^{(2)} < a_+^{(1)} \\ & b_-^{(1)} < a_+^{(2)} \\ b_-^{(2)} < & b_+^{(1)} < \underline{b}^{(1)} < b_+^{(2)} \end{array}$$

holds.

Let us consider now the ∞-shaped regions

$$\mathcal{A}^i := \{(x,y) : x > 0\,,\ c^{(i)} \le H^{(i)}(x,y) \le c_s^{(i)}\}, \quad \text{for } i = 1,2,$$

which are bounded by homoclinics $\mathcal{O}_l^{(i)}$ and $\mathcal{O}_r^{(i)}$.

As previously observed, the level line $H^{(i)}(x,y) = c^{(i)}$ has two components which are closed orbits contained in the regions $\mathcal{W}_l^{(i)}$ and $\mathcal{W}_r^{(i)}$, respectively. We set, for $i = 1,2$,

$$\Gamma_l^{(i)} := \{(x,y) : 0 < x < x_s^{(i)}\,,\ H^{(i)}(x,y) = c^{(i)}\} \subset \mathcal{W}_l^{(i)},$$

$$\Gamma_r^{(i)} := \{(x,y) : x > x_s^{(i)}\,,\ H^{(i)}(x,y) = c^{(i)}\} \subset \mathcal{W}_r^{(i)}$$

and denote by $\tau_l^{(i)}$ and $\tau_r^{(i)}$ the fundamental periods of the orbits $\Gamma_l^{(i)}$ and $\Gamma_r^{(i)}$, respectively.

The sets $\mathcal{A}^1$ and $\mathcal{A}^2$ intersects into six rectangular regions that we denote by $\mathfrak{a}_\pm, \mathfrak{b}_\pm, \mathfrak{c}_\pm$, respectively, labelling from left to right and using the sign $+$ or $-$ according to the fact that the region is contained in the upper or lower half-plane (see Figure 5).

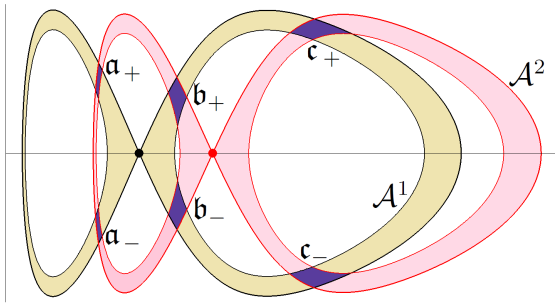

Figure 5: An example of intersection of $\mathcal{A}^1$ with $\mathcal{A}^2$ producing the six rectangular regions $\mathfrak{a}_\pm, \mathfrak{b}_\pm, \mathfrak{c}_\pm$.

Each one of the six regions introduced above can be "orientated" in two different manners. By an orientation of a topological rectangle $\mathcal{R}$, we mean the selection of two opposite sides whose union is denoted by $\mathcal{R}^-$. The two components of $\mathcal{R}^-$ are conventionally called the left and the right side (the order according to which we select to associate the terms "right" or "left" with the two sides of $\mathcal{R}^-$ is not relevant). The pair $(\mathcal{R}, \mathcal{R}^-)$ is called an *oriented rectangle*.

Now, let $\mathcal{R}$ be any of the $\mathfrak{a}_\pm, \mathfrak{b}_\pm, \mathfrak{c}_\pm$. We observe that we can give a natural orientation to the region $\mathcal{R}$ in two different manners, by choosing as $\mathcal{R}^-$ the two intersection of $\mathcal{R}$ with $H^{(1)} = c^{(1)}$ and with $H^{(1)} = c_s^{(1)}$ or the two intersection

of $\mathcal{R}$ with $H^{(2)} = c^{(2)}$ and with $H^{(2)} = c_s^{(2)}$. The corresponding oriented rectangle $(\mathcal{R}, \mathcal{R}^-)$ will be denoted as $\overset{\smile}{\mathcal{R}}$ in the former case and as $\overset{\frown}{\mathcal{R}}$ in the latter one. For example and with reference to Figure 5, the oriented rectangle $\overset{\frown}{\mathfrak{b}}_-$ is the region $\mathfrak{b}_-$ (center-below) in which we have selected as a couple of opposite sides forming $\mathfrak{b}_-^-$ the intersections of $\mathfrak{b}_-$ with the level lines $H^{(2)} = c^{(2)}$ and $H^{(2)} = c_s^{(2)}$. Analogously, the oriented rectangle $\overset{\smile}{\mathfrak{c}}_+$ is the region $\mathfrak{c}_+$ (upper-right) in which we have selected as a couple of opposite sides forming $\mathfrak{c}_+^-$ the intersections of $\mathfrak{c}_+$ with the level lines $H^{(1)} = c^{(1)}$ and $H^{(1)} = c_s^{(1)}$.

At this point we are ready to introduce a dynamical aspect, by supposing that we switch periodically between the two systems associated with the Hamiltonians $H^{(1)}$ and $H^{(2)}$. More in detail, we consider the non-autonomous second-order scalar equation

$$\ddot{x} + g(t, x) = 0 \tag{12}$$

and also the associated first order system

$$\begin{cases} \dot{x} = y \\ \dot{y} = -g(t, x) \end{cases} \tag{13}$$

in the right-half plane $x > 0$, where $g : \mathbb{R} \times \mathbb{R}_0^+ \to \mathbb{R}$ is T-periodic in the t-variable and such that

$$g(t, x) := \begin{cases} g_1(x), & \text{for } 0 \le t < T_1 \\ g_2(x), & \text{for } T_1 \le t < T_1 + T_2 = T, \end{cases} \tag{14}$$

where

$$g_i(x) := \frac{\partial H^{(i)}}{\partial x}(x, y), \quad \text{for } i = 1, 2.$$

Equation (13) is a switched system (see [2] and the references therein) and its associated Poincaré map Φ can be decomposed as

$$\Phi = \Phi_2 \circ \Phi_1$$

where Φ_i is the Poincaré map on the time-interval $[0, T_i]$ associated with the system

$$\begin{cases} \dot{x} = y \\ \dot{y} = -g_i(x) \end{cases} \tag{15}$$

for $i = 1, 2$.

Notice that, by the particular nature of the switched system (13), we can equivalently study the Poincaré map

$$\Phi = \Phi_1 \circ \Phi_2.$$

Indeed, in this latter case, we consider just a shift in time of the solutions.

4. Main result

After this preliminary discussion, we are now in position to state our main result which reads as follows.

THEOREM 4.1. *For any integer $m \geq 2$, there are T_1^* and $T_2^* > 0$ such that for each $T_1 > T_1^*$ and $T_2 > T_2^*$, the Poincaré map Φ induces chaotic dynamics on m symbols in each of the sets $\mathfrak{a}_\pm$, $\mathfrak{b}_\pm$ and $\mathfrak{c}_\pm$. Moreover, the result is robust in the sense that it is stable for small perturbations of system* (13).

Our definition of chaotic dynamics is linked to the concept of chaos according to Block and Coppel [1, 4], with a special emphasis to the presence of periodic points. More precisely, we say that a continuous and one-to-one map ψ induces chaotic dynamics on m symbols in a set $\mathcal{R}$ if there exists m pairwise disjoint compact subsets $K_1, \dots, K_m$ of $\mathcal{R}$ such that for each two-sides sequence $(s_i)_{i\in\mathbb{Z}}$ of m symbols there exists a trajectory $x_{i+1} = \psi(x_i)$ of ψ such that $x_i \in K_{s_i}$ for each $i \in \mathbb{Z}$. Moreover, if the sequence of symbols $(s_i)_{i\in\mathbb{Z}}$ is a k-periodic sequence, then also the sequence of points $(x_i)_{i\in\mathbb{Z}}$ is k-periodic. As a consequence of this definition, we have also that there exists a compact invariant set $\Lambda \subset \mathcal{R}$ having the set of periodic points of ψ as dense subset such that $\psi|_\Lambda$ is topologically semiconjugate (by a continuous and surjective map h) to the full shift automorphism on m-symbols $\sigma : \Sigma_m \to \Sigma_m := \{1, \dots, m\}^{\mathbb{Z}}$. Moreover, for each k-periodic two-sided sequence $\mathtt{s} := (s_i)_{i\in\mathbb{Z}}$, the set $h^{-1}(\mathtt{s})$ contains a k-periodic point of ψ (see [13, 16, 17]).

The proof of Theorem 4.1 is based on a variant of the theory of *topological horseshoes* [10], as developed in [16, 17]. In the first part of the next section we recall the basic tools and definitions that we are going to use.

5. Technical estimates and proof of the main result

Let $\widehat{\mathcal{M}} := (\mathcal{M}, \mathcal{M}^-)$ and $\widehat{\mathcal{N}} := (\mathcal{N}, \mathcal{N}^-)$ be oriented rectangles and let ψ be a continuous map. Let also m be a positive integer. We say that the triplet $(\widehat{\mathcal{M}}, \widehat{\mathcal{N}}, \psi)$ has the SAP (stretching along the paths) property with crossing number m, if there exist $K_1, \dots, K_m$ pairwise disjoint compact subsets of $\mathcal{M}$ such that any path γ in $\mathcal{M}$ connecting the two components of $\mathcal{M}^-$ possesses m sub-paths $\gamma_1, \dots \gamma_m$ with γ_i in K_i such that $\psi \circ \gamma_i$ is a path in $\mathcal{N}$ connecting the two components of $\mathcal{N}^-$. When this situation occurs, we write

$$\psi : \widehat{\mathcal{M}} \overset{\curvearrowright}{\Rightarrow}^m \widehat{\mathcal{N}}.$$

We avoid mentioning the apex m when $m = 1$.

The above property is compatible with composition of maps, indeed we have that:

$$\phi : \widehat{\mathcal{L}} \overset{\curvearrowright}{\Rightarrow}^k \widehat{\mathcal{M}},\ \psi : \widehat{\mathcal{M}} \overset{\curvearrowright}{\Rightarrow}^m \widehat{\mathcal{N}} \implies \psi \circ \phi : \widehat{\mathcal{L}} \overset{\curvearrowright}{\Rightarrow}^{km} \widehat{\mathcal{N}}.$$

The SAP property will be applied to prove the existence of complex dynamics for the Poincaré map, using the following result.

LEMMA 5.1. *Let $\widehat{\mathcal{R}} := (\mathcal{R}, \mathcal{R}^-)$ be an oriented rectangle and $\psi : \mathcal{R} \to \mathbb{R}^2$ be a continuous and one-to-one map. Suppose that*

$$\psi : \widehat{\mathcal{R}} \overset{\Rightarrow}{\hookrightarrow}^m \widehat{\mathcal{R}},$$

for some $m \geq 2$. Then ψ induces chaotic dynamics on m symbols on the set $\mathcal{R}$.

See [13, 16, 17, 18] for the general theory.

REMARK 5.2: A byproduct of Lemma 5.1 implies the existence of at least m fixed points for ψ in $\mathcal{R}$. More precisely, each of the pairwise disjoint compact sets $K_1 \ldots, K_m$, involved in the definition of $\psi : \widehat{\mathcal{R}} \overset{\Rightarrow}{\hookrightarrow}^m \widehat{\mathcal{R}}$, contains at least one fixed point of ψ.

The hypothesis of injectivity for the map ψ is not mandatory and the theory can be developed for arbitrary continuous maps. However, assuming ψ one-to-one is useful in order to have a semiconjugation with the Bernoulli shift on two-sided sequences (see [13] for a general discussion on this aspect). Since we apply this technique to the Poincaré map associated with a locally Lipschitz continuous differential system, the hypothesis of injectivity will be always satisfied. ◁

Now we are going to describe the crossing relationships involving the sets $\breve{\mathfrak{a}}_\pm$, $\breve{\mathfrak{b}}_\pm$, $\breve{\mathfrak{c}}_\pm$ and the dual ones $\widehat{\mathfrak{a}}_\pm$, $\widehat{\mathfrak{b}}_\pm$, $\widehat{\mathfrak{c}}_\pm$ by the maps Φ_i.

LEMMA 5.3. *Given any positive integer ℓ_1, it holds that*

$$\Phi_1 : \breve{\mathfrak{a}}_+ \overset{\Rightarrow}{\hookrightarrow}^{\ell_1} \widehat{\mathfrak{a}}_-,$$

provided that $T_1 > \ell_1 \tau_l^{(1)}$.

Proof. Let $\gamma : [0,1] \to \mathfrak{a}_+$ be a (continuous) map such that $\gamma(0) \in \Gamma_l^{(1)}$ and $\gamma(1) \in \mathcal{O}_l^{(1)}$. Equivalently, $H^{(1)}(\gamma(0)) = c^{(1)}$ and $H^{(1)}(\gamma(1)) = c_s^{(1)}$. We examine the evolution of the set $\bar{\gamma} := \gamma([0,1])$ along the Poincaré map Φ_1. Observe that Φ_1 is associated with the system

$$\dot{x} = y, \quad \dot{y} = -g_1(x) \tag{16}$$

on the time-interval $[0, T_1]$.
Along the proof, we denote by $\zeta(t, z_0) = (x(t, z_0), y(t, z_0))$ the solution of (16) satisfying the initial condition $\zeta(0) = z_0$. By definition, $\Phi_1(z_0) = \zeta(T_1, z_0)$, for any $z_0 \in \mathbb{R}_0^+ \times \mathbb{R}$.

The point $\gamma(1)$ belongs to the homoclinic trajectory and therefore it remains on $\mathcal{O}_l^{(1)}$ for all the forward time, moving in the upper phase-plane from left to

right but never meeting the saddle point $x_s^{(1)}$. As a consequence, $x(t,\gamma(1)) < x_s^{(1)}$ and $y(t,\gamma(1)) > 0$ for all $t \in [0,T_1]$. On the other hand, the point $\gamma(0)$ belongs to the periodic orbit $\Gamma_l^{(1)}$ of period $\tau_l^{(1)}$ and therefore, if $T_1 > \tau_l^{(1)}$, it makes at least ℓ_1 complete turns (in the clockwise sense) around the center $(a^{(1)},0)$ in the interval $[0,T_1]$.

If we introduce a polar coordinate system (θ,ρ), starting from the half-line $\{(x,0) : x < a^{(1)}\}$ and counting positive rotations in the clockwise sense, we have that $0 < \theta(\gamma(s)) < \pi$ for all $s \in [0,1]$ and then we define the sets

$$K_j := \{z \in \mathfrak{a}_+ \,:\, (2j-1)\pi < \theta(\Phi^{(1)}(z)) < 2j\pi\}, \quad \text{for } j = 1,\dots,\ell_1.$$

By the previous observation about the movement of the points $\gamma(1)$ and $\gamma(0)$ under the influence of the dynamical system of (16), we know that $\theta(\Phi_1(\gamma(1))) < \pi$, while $\theta(\Phi_1(\gamma(0))) > 2j\ell_1\pi$.

A simple continuity argument on the map $[0,1] \ni s \mapsto \theta(\Phi_1(\gamma(s)))$, implies the existence of ℓ_1 pairwise disjoint intervals $[\alpha_j,\beta_j] \subset [0,1]$ such that $(2j-1)\pi \le \theta(\Phi_1(\gamma(s))) \le 2j\pi$ for all $s \in [\alpha_j,\beta_j]$ with $\theta(\Phi_1(\gamma(\alpha_j)) = 2j\pi$ and $\theta(\Phi_1(\gamma(\beta_j)) = (2j-1)\pi$.
By definition, the path $\Phi_1 \circ \gamma$ restricted to the interval $[\alpha_j,\beta_j]$ is contained in the half-annulus

$$\mathcal{A}^1 \cap \{(x,y) : 0 < x < x_s^{(1)}\,,\ y \le 0\}$$

and therefore, it crosses the rectangle $\mathfrak{a}_-$ intersecting both components of $\mathfrak{a}_-^-$. Using again an elementary continuity argument of the map $s \mapsto \Phi_1(\gamma(s))$, for each $j = 1,\dots,\ell_1$, we determine a sub-interval $[\alpha_j',\beta_j'] \subset [\alpha_j,\beta_j]$ such that, $\Phi_1(\gamma(s)) \in \mathfrak{a}_-$ for all $s \in [\alpha_j',\beta_j']$. Moreover, $\Phi_1(\gamma(\alpha_j'))$ and $\Phi_1(\gamma(\beta_j'))$ belong to different components of $\mathfrak{a}_-$. Note also that, by construction, $\gamma(s) \in K_j$ for all $s \in [\alpha_j',\beta_j']$. We have thus verified the SAP property for $(\overset{\smile}{\mathfrak{a}}_+, \overset{\frown}{\mathfrak{a}}_-, \Phi_1)$ with crossing number ℓ_1, provided that $T_1 > \ell_1\tau_l^{(1)}$ and the proof is complete. □

At this point, we can repeat the same argument of the proof of Lemma 5.3 and consider all the possible combinations between the oriented rectangles and the maps Φ_i. We can summarize these conclusions by the following lemmas where the times τ_i^* can be easily determined from the periods of the closed orbits $\Gamma_l^{(i)}$ and $\Gamma_s^{(i)}$.

LEMMA 5.4. *There exist times τ_1^* and τ_2^*, such that, for any positive integers ℓ_1,ℓ_2 it holds that:*

$\Phi_1 : \overset{\smile}{\mathfrak{a}}_\pm \overset{\ell_1}{\twoheadrightarrow} \overset{\frown}{\mathfrak{a}}_\pm$, $\overset{\smile}{\mathfrak{b}}_\pm \overset{\ell_1}{\twoheadrightarrow} \overset{\frown}{\mathfrak{b}}_\pm$, $\overset{\frown}{\mathfrak{c}}_\pm$, $\overset{\smile}{\mathfrak{c}}_\pm \overset{\ell_1}{\twoheadrightarrow} \overset{\frown}{\mathfrak{b}}_\pm$, $\overset{\frown}{\mathfrak{c}}_\pm$,
provided that $T_1 > \ell_1\tau_1^*$.

$\Phi_2 : \overset{\frown}{\mathfrak{a}}_\pm \overset{\ell_2}{\twoheadrightarrow} \overset{\smile}{\mathfrak{a}}_\pm$, $\overset{\smile}{\mathfrak{b}}_\pm$, $\overset{\frown}{\mathfrak{b}}_\pm \overset{\ell_2}{\twoheadrightarrow} \overset{\smile}{\mathfrak{a}}_\pm$, $\overset{\smile}{\mathfrak{b}}_\pm$, $\overset{\frown}{\mathfrak{c}}_\pm \overset{\ell_2}{\twoheadrightarrow} \overset{\smile}{\mathfrak{c}}_\pm$,
provided that $T_2 > \ell_2\tau_2^*$.

In the above lemma, when we write a condition such as $\smile_{\pm} \overset{\ell}{\nrightarrow} \frown_{\pm}$, we mean that all the four possibilities in the choice of $\pm$ for the domain and codomain are possible.

The content of Lemma 5.4 is explained by means of Figure 6 and Figure 7.

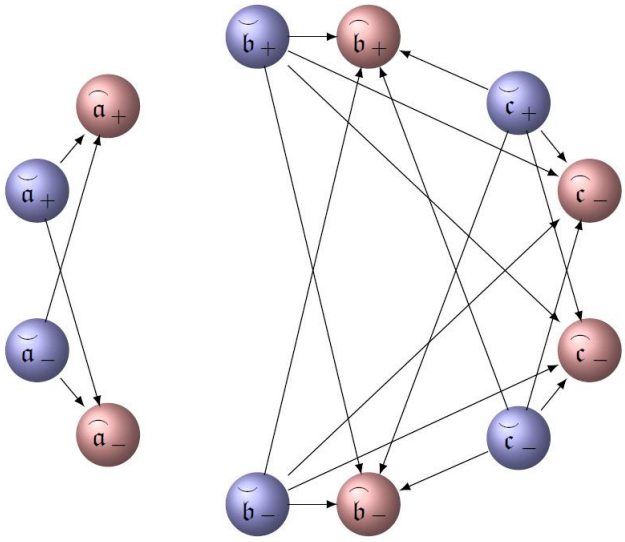

Figure 6: This graph represents all the possible connections by the partial Poincaré map Φ_1. The arrows correspond to the $\overset{\ell}{\nrightarrow}$ symbol. The integer ℓ_1 is not indicated but it can be arbitrarily chosen provided that $T_1 > \ell_1 \tau_1^*$.

Now, we are in position to conclude with the proof of our main result.

Proof of Theorem 4.1. Using Lemma 5.4 along with Lemma 5.1 we can guarantee that the Poincaré map $\Phi = \Phi_2 \circ \Phi_1$, as well as $\Phi = \Phi_1 \circ \Phi_2$ induces chaotic dynamics on any finite number of symbols, provided that T_1 and T_2 are large enough.

From the proof of Lemma 5.3 it is clear that the result is stable by small perturbations and the same holds for all the connections considered in Lemma 5.4.

In our case we have several possibilities of producing chaotic dynamics on $m \geq 2$ symbols on a rectangular region $\mathcal{R}$ chosen among the sets $\mathfrak{a}_{\pm}$, $\mathfrak{b}_{\pm}$ and $\mathfrak{c}_{\pm}$. In order to explain better how these possibilities arise, we fix out attention only on the Poincaré map $\Phi = \Phi_2 \circ \Phi_1$ (the other case is treated in a similar manner).

A first and more natural case is to take $\max\{\ell_1, \ell_2\} \geq 2$, so that

$$m = \ell_1 \times \ell_2 \geq 2$$

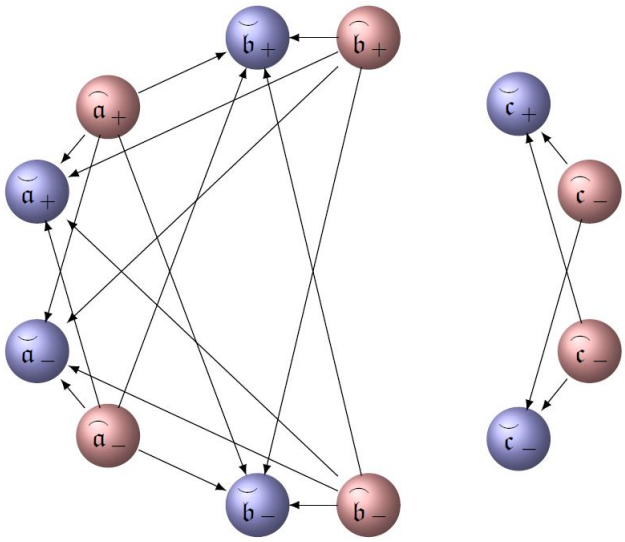

Figure 7: This graph represents all the possible connections by the partial Poincaré map Φ_2. The arrows correspond to the $\twoheadrightarrow$ symbol. The integer ℓ_2 is not indicated but it can be arbitrarily chosen provided that $T_2 > \ell_2 \tau_2^*$.

and, considering the connections described in Lemma 5.4, we immediately see that Lemma 5.1 can be applied for $\widehat{\mathcal{R}}$ any of the sets $\breve{\mathfrak{a}}_\pm$, $\breve{\mathfrak{b}}_\pm$, $\breve{\mathfrak{c}}_\pm$. However, a more careful analysis of the connection diagrams shows that in these sets the SAP property with crossing number greater or equal than two can be obtained also in the case when $\ell_1 = \ell_2 = 1$ (this may be more interesting from the point of view of the applications because we need a lesser restriction on the period). In fact, the following connections are available

$$\begin{aligned}
&\breve{\mathfrak{a}}_+ \twoheadrightarrow \hat{\mathfrak{a}}_+ \twoheadrightarrow \breve{\mathfrak{a}}_+\,, && \breve{\mathfrak{a}}_+ \twoheadrightarrow \hat{\mathfrak{a}}_- \twoheadrightarrow \breve{\mathfrak{a}}_+\\
&\breve{\mathfrak{a}}_- \twoheadrightarrow \hat{\mathfrak{a}}_- \twoheadrightarrow \breve{\mathfrak{a}}_-\,, && \breve{\mathfrak{a}}_- \twoheadrightarrow \hat{\mathfrak{a}}_+ \twoheadrightarrow \breve{\mathfrak{a}}_-\\
&\breve{\mathfrak{b}}_+ \twoheadrightarrow \hat{\mathfrak{b}}_+ \twoheadrightarrow \breve{\mathfrak{b}}_+\,, && \breve{\mathfrak{b}}_+ \twoheadrightarrow \hat{\mathfrak{b}}_- \twoheadrightarrow \breve{\mathfrak{a}}_+\\
&\breve{\mathfrak{b}}_- \twoheadrightarrow \hat{\mathfrak{b}}_- \twoheadrightarrow \breve{\mathfrak{b}}_-\,, && \breve{\mathfrak{b}}_- \twoheadrightarrow \hat{\mathfrak{b}}_+ \twoheadrightarrow \breve{\mathfrak{b}}_-\\
&\breve{\mathfrak{c}}_+ \twoheadrightarrow \hat{\mathfrak{c}}_+ \twoheadrightarrow \breve{\mathfrak{c}}_+\,, && \breve{\mathfrak{c}}_+ \twoheadrightarrow \hat{\mathfrak{c}}_- \twoheadrightarrow \breve{\mathfrak{a}}_+\\
&\breve{\mathfrak{c}}_- \twoheadrightarrow \hat{\mathfrak{c}}_- \twoheadrightarrow \breve{\mathfrak{c}}_-\,, && \breve{\mathfrak{c}}_- \twoheadrightarrow \hat{\mathfrak{c}}_+ \twoheadrightarrow \breve{\mathfrak{c}}_-
\end{aligned}$$

and therefore, we find that

$$\Phi : \breve{\mathfrak{a}}_\pm \twoheadrightarrow^2 \breve{\mathfrak{a}}_\pm\,, \qquad \breve{\mathfrak{b}}_\pm \twoheadrightarrow^2 \breve{\mathfrak{b}}_\pm\,, \qquad \breve{\mathfrak{c}}_\pm \twoheadrightarrow^2 \breve{\mathfrak{c}}_\pm\,.$$

In the last formula we use the convention that $[]_\pm \twoheadrightarrow []_\pm$ means that only the two possibilities $[]_+ \twoheadrightarrow []_+$ and $[]_- \twoheadrightarrow []_-$ are available.

The situation becomes more complicated and interesting if we consider the iterates of the map Φ. For instance, for the map Φ^2, and taking $\widehat{\mathcal{R}} = \breve{\mathfrak{a}}_+$ as a starting set, new connections are available, such as

$$\breve{\mathfrak{a}}_+ \twoheadrightarrow^2 \breve{\mathfrak{b}}_\pm \twoheadrightarrow^2 \breve{\mathfrak{a}}_+ \text{ and } \breve{\mathfrak{a}}_+ \twoheadrightarrow^2 \breve{\mathfrak{a}}_\pm \twoheadrightarrow^2 \breve{\mathfrak{a}}_+ .$$

Hence, counting all the possible connections for Φ^2, we obtain that

$$\Phi^2 : \breve{\mathfrak{a}}_+ \twoheadrightarrow^{16} \breve{\mathfrak{a}}_+.$$

In fact, from $\breve{\mathfrak{a}}_+$ we come back again to $\breve{\mathfrak{a}}_+$ by Φ^2 passing through the four sets $\breve{\mathfrak{a}}_\pm$ and $\breve{\mathfrak{b}}_\pm$ and, each time we apply Φ we have two itineraries available. Similar combinations occur for the other oriented rectangles. □

6. Final remarks

The existence of chaos in differential systems which are obtained as periodic perturbations of planar autonomous systems exhibiting homoclinic or heteroclinic trajectories is a well established fact (see [15, 8]). The methods of proof applied in those situations, such as the Melnikov method, usually permit to enter in the framework of Smale's horseshoe (cf. [19] and [14]) which guarantees the existence of a compact invariant set for the Poincaré map Φ, where Φ is *topologically conjugate* to the Bernoulli shift on a certain set of symbols. Our result provides a weaker form of chaos since only the semiconjugation is proved. On the other hand, in the concrete applications, some explicit knowledge of the homoclinic (or heteroclinic) solution, in terms of its analytic expression is often needed. A typical example is given by the classical periodically perturbed Duffing equation

$$\ddot{x} - x + x^3 = \varepsilon p(\omega t), \tag{17}$$

where the Melnikov function can be explicitly defined (see [8]) thanks to the knowledge of the analytic expression of the homoclinic solutions of

$$\dot{x} = y, \quad \dot{y} = x - x^3.$$

In the model studied in the present paper, two difficulties arise: first, we do not know an explicit form of the homoclinic solutions of system (9) and, secondly, the periodic perturbation leading to (12) from (8), which corresponds to a variation of the form $B_0 \mapsto B_0(t)$ in (10), appears to be more complicated than the perturbation considered in equation (17). Our approach, even if applied to the simplified situation of a stepwise function $B_0(t)$, allows to prove the presence

of chaotic dynamics using only few geometric information on the geometry of the level curves of the associated energy functions. As already shown in [12] and in [11, Section 8], the choice of a stepwise coefficient has the advantage not only to simplify some technical estimates, but also to put in evidence the presence of interesting bifurcation phenomena for the solutions of the nonlinear equations which are involved.

Acknowledgements

Work performed under the auspices of Gruppo Nazionale per l'Analisi Matematica, la Probabilità e le loro Applicazioni (GNAMPA) of the Istituto Nazionale di Alta Matematica (INdAM) and supported by PRID "Dynamical Systems" of the University of Udine. A preliminary version of this research was presented by O.G. at the conference *GEDO2018*, Ancona, September 27-29, 2018.

References

[1] B. Aulbach and B. Kieninger, *On three definitions of chaos*, Nonlinear Dyn. Syst. Theory **1** (2001), no. 1, 23–37.
[2] A. Bacciotti, *Bounded-input-bounded-state stabilization of switched processes and periodic asymptotic controllability*, Kybernetika (Prague) **53** (2017), no. 3, 530–544.
[3] F. Battelli and K. J. Palmer, *Chaos in the Duffing equation*, J. Differential Equations **101** (1993), no. 2, 276–301.
[4] L. S. Block and W. A. Coppel, *Dynamics in one dimension*, Lecture Notes in Mathematics, vol. 1513, Springer-Verlag, Berlin, 1992.
[5] B. Cambon, X. Leoncini, M. Vittot, R. Dumont, and X. Garbet, *Chaotic motion of charged particles in toroidal magnetic configurations*, Chaos **24** (2014), no. 3, 033101, 11.
[6] W. M. Elsasser, *Induction effects in terrestrial magnetism part I. theory*, Phys. Rev. **69** (1946), 106–116.
[7] O. Gjata and F. Zanolin, *An example of chaotic dynamics for charged particles in a magnetic field*, (submitted) (2020).
[8] J. Guckenheimer and P. Holmes, *Nonlinear oscillations, dynamical systems, and bifurcations of vector fields*, Applied Mathematical Sciences, vol. 42, Springer-Verlag, New York, 1990, Revised and corrected reprint of the 1983 original.
[9] J. Kennedy, S. Koçak, and J. A. Yorke, *A chaos lemma*, Amer. Math. Monthly **108** (2001), no. 5, 411–423.
[10] J. Kennedy and J. A. Yorke, *Topological horseshoes*, Trans. Amer. Math. Soc. **353** (2001), no. 6, 2513–2530.
[11] J. López-Gómez, P. Omari, and S. Rivetti, *Bifurcation of positive solutions for a one-dimensional indefinite quasilinear neumann problem*, Nonlinear Analysis **155** (2017), 1–51.

[12] J. López-Gómez, A. Tellini, and F. Zanolin, *High multiplicity and complexity of the bifurcation diagrams of large solutions for a class of superlinear indefinite problems*, Commun. Pure Appl. Anal. **13** (2014), 1–73.
[13] A. Medio, M. Pireddu, and F. Zanolin, *Chaotic dynamics for maps in one and two dimensions: a geometrical method and applications to economics*, Internat. J. Bifur. Chaos Appl. Sci. Engrg. **19** (2009), no. 10, 3283–3309.
[14] J. Moser, *Stable and random motions in dynamical systems*, Princeton University Press, Princeton, N. J.; University of Tokyo Press, Tokyo, 1973, With special emphasis on celestial mechanics, Hermann Weyl Lectures, the Institute for Advanced Study, Princeton, N. J, Annals of Mathematics Studies, No. 77.
[15] K. J. Palmer, *Transversal heteroclinic points and Cherry's example of a nonintegrable Hamiltonian system*, J. Differential Equations **65** (1986), no. 3, 321–360.
[16] D. Papini and F. Zanolin, *Fixed points, periodic points, and coin-tossing sequences for mappings defined on two-dimensional cells*, Fixed Point Theory Appl. (2004), no. 2, 113–134.
[17] D. Papini and F. Zanolin, *On the periodic boundary value problem and chaotic-like dynamics for nonlinear Hill's equations*, Adv. Nonlinear Stud. **4** (2004), no. 1, 71–91.
[18] A. Pascoletti, M. Pireddu, and F. Zanolin, *Multiple periodic solutions and complex dynamics for second order ODEs via linked twist maps*, The 8th Colloquium on the Qualitative Theory of Differential Equations, Proc. Colloq. Qual. Theory Differ. Equ., vol. 8, Electron. J. Qual. Theory Differ. Equ., Szeged, 2008, pp. No. 14, 32.
[19] S. Smale, *Differentiable dynamical systems*, Bull. Amer. Math. Soc. **73** (1967), no. 6, 747–817.

Authors' addresses:

Oltiana Gjata
Department of Mathematics, Computer Science and Physics,
University of Udine
Via delle Scienze 206, 33100 Udine, Italy
E-mail: gjata.oltiana@spes.uniud.it

Fabio Zanolin
Department of Mathematics, Computer Science and Physics
University of Udine
Via delle Scienze 206, 33100 Udine, Italy
E-mail: fabio.zanolin@uniud.it

Received February 29, 2020
Revised March 29, 2020
Accepted March 29, 2020